CI&CEQ
Chemical Industry & Chemical Engineering Quarterly

Available on line at
Association of the Chemical Engineers of Serbia *AChE*
www.ache.org.rs/CICEQ

Chem. Ind. Chem. Eng. Q. 26 (3) 227–236 (2020) CI&CEQ

JUN NIU[1]
SHUO LIU[2,3]
JING-YU XU[2,3]

[1]Petroleum Exploration and Production Research Institute of SINOPEC, Beijing, China
[2]Institute of Mechanics, Chinese Academy of Sciences, Beijing, China
[3]School of Engineering Sciences, University of Chinese Academy of Sciences, Beijing, China

SCIENTIFIC PAPER

UDC 621.928:66.07:519.87

INVESTIGATION ON SEPARATION PERFORMANCE OF VANE-TYPE GAS-LIQUID TUBE SEPARATOR

Article Highlights

- New vane-type gas-liquid separator with necking was proposed
- Electrical resistance tomography was applied for section void fraction and gas core size measurement
- Numerical simulation was validated by experimental measurement
- Influence of split ratio and gas core size on separation efficiency was investigated

Abstract

In this work, gas phase distribution characteristic and separation performance of a new vane-type gas-liquid separator were carefully investigated using electrical resistance tomography and numerical simulation. The diameter of the separator was 100 mm and the flow rate ranges from 12.0 to 23.0 m^3/h. The gas flow rate ranges from 1.2 to 4.0 m^3/h. In the experiment, electrical resistance tomography was applied to test section void fraction distribution. Coriolis mass flow meter was applied to obtain separation efficiency by testing separator exits mixture density. In the numerical simulation, full Eulerian multiphase model, together with RNG k-ε turbulent model and dispersed phase zero equation models were applied. Results show that the vane-type gas-liquid separator's performance is influenced by gas core size. The separator performs well in all the cases, considering separation efficiency is over 85%, and achieves nearly 100% through adjustment of split ratio. All these findings are beneficial for vane-type gas-liquid separator design and optimization.

Keywords: gas-liquid separation, separation efficiency, numerical simulation, flow experiment, tube separator, process design.

Gas-liquid separation is an important process in various fields such as crude extraction, molten salt reactors or air demisters. Different to air demisters, liquid phase exists continuously in fields of crude extraction and molten salt reactors, and the bubble or gas phase is the minority. In the field of petroleum and mining engineering, gas-liquid separation is commonly applied in the preprocess procedure which provides preconditions for further downstream process. Through years of development, the philosophy of gas-liquid separation technology has reformed from gravity separation to centrifugal separation which better fits strict space demands. Correspondingly, the type of gas-liquid separator changed from gravity-style to a compact cyclone that can be further divided into tangential-induced and axial-induced separators [1-3]. The tangential-induced cyclone gas-liquid separator has long been investigated and reformed through researchers' continuous efforts [4-7] on the mechanism and refinement methods. While the axial-induced cyclone gas-liquid separator, whose representation is the vane-type separator, has long been applied in molten salt reactors but seldom in crude extraction process techniques.

A vane-type separator is better than a tangential-induced cyclone in aspects of space demand, pressure drop and structural complexity [8]. In recent studies, researchers' interests mainly focused on the vane shape design, flow domain characters, and gas-liquid flow. Cai *et al.* [8] and Huang *et al.* [9] conduct vane shape optimization through numerical simul-

Correspondence: S. Liu, Institute of Mechanics, Chinese Academy of Sciences, Beijing, 100190, China.
E-mail: liushuo@imech.ac.cn
Paper received: 9 September, 2019
Paper revised: 6 November, 2019
Paper accepted: 12 December, 2019

https://doi.org/10.2298/CICEQ190909040N

ation. As with the investigation of flow field, Klujzo [10] investigated the relationship between pressure drop and vane parameters through both CFD simulation and experiment observation. Hoffman *et al.* [11] studied pressure distribution of recovery vanes by pressure measurement and numerical simulation. Shi and Xu [12] measured tangential, radical and axial velocity distribution of continuous phase of swirling flow field generated through straight vanes. As with gas-liquid two phase flows, Funahashi *et al.* [13] investigated characteristics of gas-water two phase swirling flows and separation performances with one-fifth scale model experiment. Yin *et al.* [14] conducted detailed research on the bubble trajectory in vane-type swirling flow field applied in molten salt reactor.

Though research works above have been done on gas-liquid separators, challenges still exist. Most works above don't pay attention to gas core size measurements. Ways to test gas core size and validate numerical simulation still needs much effort. Traditional photography may fail to tell gas core size due to the refraction of the pipe wall. In this situation, electrical resistance tomography (ERT for abbreviation) may be an ideal choice. Our previous work [16,17] presents flow characteristics of gas-liquid swirling flow fields of a new swirling vane-type using ERT. However, the flow character may change in the double-outlet separators. In this work, corresponding vane-type gas-liquid tube separator with necking was proposed and carefully studied through ERT and numerical simulation and was conducted on oil-water flow induced by guide vanes [18]. Flow experiment was operated with ERT measuring section void fraction and Coriolis mass flow meter charactering separation performance. Corresponding numerical simulation coupled Eulerian multiphase model with RNG k-ε turbulent model and dispersed zero equation models. Combining experimental results and numerical simulation, gas phase distribution in the whole flow field and separation performances can be clearly described which is beneficial for future gas-liquid tube separator optimization.

Theoretical part

Mathematical modeling

Numerical simulation work was performed on Ansys CFX. In terms of numerical mathematical modeling selection, through experimental observation, it can be seen that bubble dispersion turns into continuous gas core after the vane zone in the separator. So, the form of secondary gas phase ranges from bubble to continuous phase. On the basis of literature work on gas-liquid multiphase flow in swirling flow field [15,20,21], full Eulerian approach is an ideal choice in this condition. In the full Eulerian approach, equations for all the phases are solved. For certain phase i, in ignorance of phase change, the continuity and momentum equations are shown as Eqs. (1) and (2):

$$\frac{\partial}{\partial t}\left(\alpha_i\rho_i\right)+\nabla\left(\alpha_i\rho_i\vec{u}_i\right)=0 \tag{1}$$

$$\frac{\partial}{\partial t}\left(\alpha_i\rho_i\vec{u}_i\right)+\nabla\left(\alpha_i\rho_i\vec{u}_i\vec{u}_i\right)=-\alpha_i\nabla p+\nabla\overline{\overline{\tau}}_i+\alpha_i\rho_i\vec{g}+ +\sum_{i=1}^{n}K_{ji}\left(\vec{u}_j-\vec{u}_i\right)+ +\alpha_i\rho_i\left(\vec{F}_i+\vec{F}_{lift,i}+\vec{F}_{vm,i}\right) \tag{2}$$

where i represents i^{th} phase, α represents volume fraction, ρ_i represents density and $\vec{u}_i$ is the velocity, $\overline{\overline{\tau}}_i$ is the i^{th} phase stress-strain tensor. K_{ij} represents water-bubble exchange coefficient, which characterizes drag force. It can be written in form of Eq. (3), where τ_p is particulate relaxation time, written in form of Eq. (4). For Schiller and Naumann models, drag function f is written as Eq. (5), where Re is the relative Reynolds number between the water and bubble, C_D is 0.44 for Re larger than 1000, and 24(1+ +0.15$Re^{0.687}$)/Re when Re is smaller than 1000:

$$K_{ij}=\frac{\alpha_j\alpha_i\rho_i f}{\tau_i} \tag{3}$$

$$\tau_i=\frac{\rho_i d_i^2}{18\mu_j} \tag{4}$$

$$f=\frac{C_D Re}{24} \tag{5}$$

$\vec{F}_i$ is the body force originating from the interaction with the dispersed phase, such as surface tension. $\vec{F}_{lift,i}$ is the lift force originating from velocity gradients of the primary-phase flow field, and can be shown in Eq. (6). $\vec{F}_{vm,i}$ is the virtual mass force originating from secondary phase i accelerating part of primary phase j around the accelerating particles, and can be shown as Eq. (7):

$$\vec{F}_{lift,i}=-0.5\rho_i\alpha_i\left(\vec{u}_j-\vec{u}_i\right)\times\left(\nabla\times\vec{u}_j\right) \tag{6}$$

$$\vec{F}_{vm,i}=0.5\alpha_i\rho_j\left(\frac{d_j\vec{u}_j}{dt}-\frac{d_i\vec{u}_i}{dt}\right) \tag{7}$$

As with turbulent models, phase-dependence models are first to be applied for the gas and liquid phases. Considering the main phase is the water in the swirling flow, on the basis of Escue and Cui's

work [22] and Sadi *et al.* work [23], together with the previous research [17] on the turbulent modeling selection for vane type swirling flow field under relatively low swirl conditions, RNG k-ε model performs better under experimental operating conditions in terms of tangential velocity distribution and gas core simulation. As a consequence, the turbulent model of the water phase is confirmed as RNG k-ε model as shown in Eqs. (8) and (9):

$$\frac{\partial}{\partial t}(\rho k)+\frac{\partial}{\partial x_j}(\rho k u_i)= \\ =\frac{\partial}{\partial x_j}\left(\alpha_k \mu_{eff}\frac{\partial k}{\partial x_j}\right)+G_k+G_b-\rho\varepsilon-Y_M+S_K \tag{8}$$

$$\frac{\partial}{\partial t}(\rho\varepsilon)+\frac{\partial}{\partial x_j}(\rho\varepsilon u_i)=\frac{\partial}{\partial x_j}\left(\alpha_\varepsilon \mu_{eff}\frac{\partial \varepsilon}{\partial x_j}\right)+ \\ +G_{1\varepsilon}\frac{\varepsilon}{k}(G_k+G_{3\varepsilon}G_b)-G_{2\varepsilon}\rho\frac{\varepsilon^2}{k}-R_\varepsilon+S_\varepsilon \tag{9}$$

in which G_k represents the generation of turbulence kinetic energy due to mean velocity gradients; G_b is the generation of turbulence kinetic energy due to buoyancy; Y_M represents the contribution of the fluctuating dilatation in compressible turbulence to the overall dissipation rate. The quantities are the inverse effective Prandtl numbers for k and ε, respectively. S_k and S_ε are user-defined source terms.

For turbulent model of discrete phase, dispersed phase zero equation (DPZE) model is an ideal choice [15], which connects kinematic eddy viscosity of continuous and discrete phases by turbulent Prandtl number. The model can be characterized by Eq. (10):

$$\mu_{tb}=\frac{\rho_b}{\rho_a}\frac{\mu_{ta}}{\sigma_a} \tag{10}$$

where μ_{tb} refers to dispersed phase kinematic eddy viscosity, μ_{ta} refers to continuous phase kinematic eddy viscosity, and σ_a is the turbulent Prandtl number. Further, bubble-induced turbulence on the continuous phase can be characterized by the Sato enhancement model which divides continuous turbulent viscosity into inherent viscosity and bubble agitation-induced viscosity.

Separator configuration

The configuration of the gas-liquid tube separator is shown as Figure 1 in which the separator consists of 6 parts, namely vanes, the developing tube, necking, gas collection tube, the run and the branch. The separator is a passive one without moving parts; the element to induce swirling flow is a hub with 6 fixed swirling vanes whose geometry parameter can be checked in our previous work about gas-liquid swirling flow field. After the vane zone is a section of developing tube which provides enough space for formation of a stable gas core. Innovatively, necking from 100 to 80 mm of inner diameter is placed 1 m downstream vane zone to help stabilize the gas core. In the phase collecting part, a 25 mm gas collection tube was mounted downstream of the necking with a 90° elbow to induce gas core through branch to overflow. Meanwhile, a run pipe with 65 mm inner diameter was designed for exit of the rest of the mixture fluids. Detail structural parameters of the separator are listed in Table 1. Under this separator design, gas-liquid mixture can form a stable gas core, then

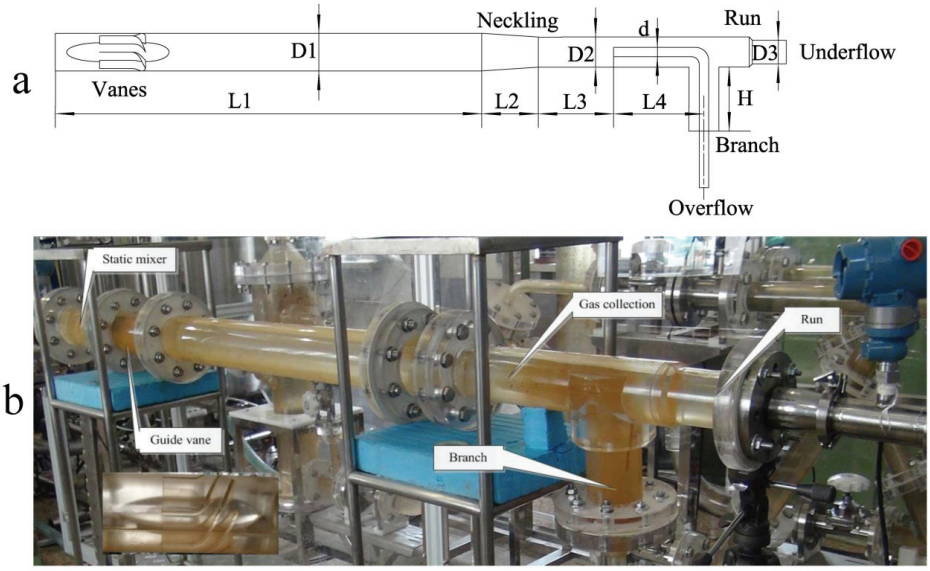

Figure 1. Separator configuration and photograph.

enter gas collection tube and exist at overflow, while the rest of the mixture exits at the run.

Table 1. Structural parameters for the separator

Structural parameter	Value, mm
d	25
D_1	100
D_3	65
D_2	80
L_1	1130
L_2	150
L_3	200
L_4	240
H	170

Geometry model and grid generation

Modeling procedure is performed on the ANSYS design modeler part. At the vane zone, the flow domain is sliced by space surface corresponding to the shape of swirling vanes. Location corresponding to the hub is hollow. Downstream to the gas phase collection part, the flow domain is divided by the branch pipe wall.

Grid generation procedure is conducted on the ICEM CFD software platform. Through O-blocking method, structural grids are created. Independent grid study was performed on 3 grid schemes: a) 652,016, b) 1,180,612 and c) 1,506,218 cells. Facet average velocity magnitude was selected as grid scheme selection criteria. Variance of scheme a to b was far larger than b to c (3.1 to 0.57%). So, scheme b was chosen to perform simulation for its usability and less calculation consumption, the size of grid ranges from 0.46 to 4.6 mm.

Boundary condition and solution settings

The fluid domain is occupied with two-phase medium, in which the water is a continuous phase, while the gas is the discrete phase. The reference pressure for the flow domain is 1 atm. Buoyant model is applied with reference density 998.1 kg/m^3, and gravity settings of -9.81 m/s^2 in the -z direction [24]. Besides, in the fluid pair model settings, 0.072 N/m surface tension coefficient is set for water-air medium. Boundary condition settings can be checked on Table 2. The entrance of the separator is set as velocity inlet and phase volume fraction from experimental measurements. Bubble mean diameter from the prediction model proposed in previous work [17] is also needed. The underflow and overflow are set as pressure outlets whose values are measured from the pressure gauge and pressure difference gauge. For vanes, due to their fixed property, they are set as a fixed wall. For the pipe wall, and branch wall, no slip conditions are chosen.

For the solution settings, high resolution advection scheme is applied in the simulation work. And residual target convergence criteria are set as 10^{-5}. In order to make the convergence better and faster, pure water phase convergence is first achieved for the separator fluid domain as the initial condition, then the bubbles are added at the entrance of the separator.

EXPERIMENTAL

Working fluids

In the experimental research work, tap water and air are applied as working fluids of the liquid phase and gas phase, respectively. Under experimental conditions (20 °C), the density of water is 998.1 kg/m^3, while the density of air is 1.29 kg/m^3. The corresponding air-water surface tension factor is 0.072 N/m.

Measuring technique and systematic error

Coriolis mass flowmeter (CMF) is applied for measurement of mixture density and mass flow rate of the overflow. Specification of CMF applied in this research is MicroMotion F050 produced by Emerson. According to literature, the maximum and minimum error is 16.83 and -13.42%. And the average error is 0.82% [19].

ERT is applied for void fraction distribution measurement in this work. It's a kind of a noninvasive industrial process tomography obtaining conductivity variations of different phases. With 16 stainless steel electrodes mounted around the testing section, phase local volume fraction (α) distribution can be obtained by Maxwell's equation:

Table 2. Comparison of split ratios numerically and experimentally

Case No.	Case parameter				Split ratio, %	
	Liquid inlet flow rate m^3/h	Gas inlet flow rate m^3/h	Pressure difference kPa	Underflow pressure kPa	Simulation result	Test result
1	23.3	1.2	-13.06	76.48	23.5	20.9
2	23.1	4	-16.35	107.4	32.8	29
3	16.3	1.2	-4.68	44.63	20.4	15.4

$$\alpha = \frac{2\sigma_1 + \sigma_2 - 2\sigma_{mc}\sigma_{mc}\dfrac{\sigma_1}{\sigma_2}}{\sigma_{mc} - \sigma_{mc}\dfrac{\sigma_1}{\sigma_2} + 2(\sigma_1 - \sigma_1)} \quad (6)$$

where σ_1 is the conductivity of the first phase, σ_1 is the conductivity of the second phase, σ_{mix} is the conductivity of the mix phase.

In terms of systematic error, according to Wang's work [25], reference error of 1% may lead up to 10% conductivity error. As a consequence, ERT should be calibrated with pure water without the gas phase before the experiment. As the reference measurement error could be controlled within 1.0%, the total relative error of void fraction is within 10%. Specification applied in the experiment is EIT 3000, whose testing parts are two planes with 16 round mounted electrodes around the pipe wall.

Experiment flow loop

The flow experiment is erected on the basis of a self-circulation flow system as is shown in Figure 2. Upstream entrance of the separator, a pressure gauge and static mixer are placed, whose specifications are SV-5 for pressure measurement and bubble dispersion, respectively. Downstream vane zone 6.4 and 8 D_1, two EIT pixels are mounted for phase distribution measurement. Next, a pressure differential gauge is connected with overflow and underflow. Then, a CMF is connected with underflow for measurement of mixture density and mass flow rate. In the flow loop, water from a water tank and air from a gas compressor get fully mixed to become bubbly dispersion flow in the static mixer, then flow through the vane zone to form swirling flow. After the flow domain is stabled, the gas core and water nearby enter the branch and flow out through overflow, while other fluids flow in the run pipe to enter the CMF. At last, the two branches confluence at the collecting tank.

Operating conditions

Operating conditions differ through variation of inlet water flow rate, inlet air flow rate and valve opening, which is rated with split ratio. In the experiment, the inlet air flow rate contains 1.2, 2.5, 4.0, and 6.0 m^3/h operating conditions, with inlet water flow rate changing from 12.0 to 23.0 m^3/h. Moreover, there are several split ratios for fixed phase flow rate.

RESULTS AND DISSCUSSION

In this research, the separation performances and relationship between operating parameters with separation efficiency is mainly investigated through experimental work, while gas phase distribution research in the separator is partially through EIT and partially CFX simulation. Hence, numerical simulation should be first validated by experimental measurement.

Validation of numerical simulation

Gas phase distribution by photograph in the whole separator, void fraction distribution at the EIT testing section, and split ratio are chosen as key parameters for comparison between numerical simulation and experimental observation.

Figure 3 illustrates 3 cases of gas phase distribution for numerical simulation and photograph, respectively. The operating condition parameter can be checked in Table 2. It can be seen that for each case,

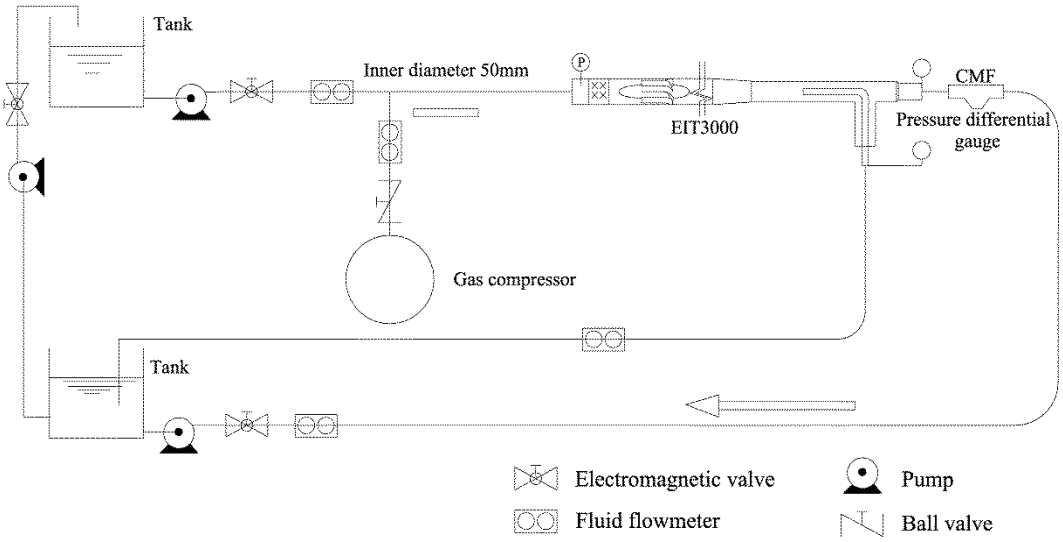

Figure 2. Flow loop system.

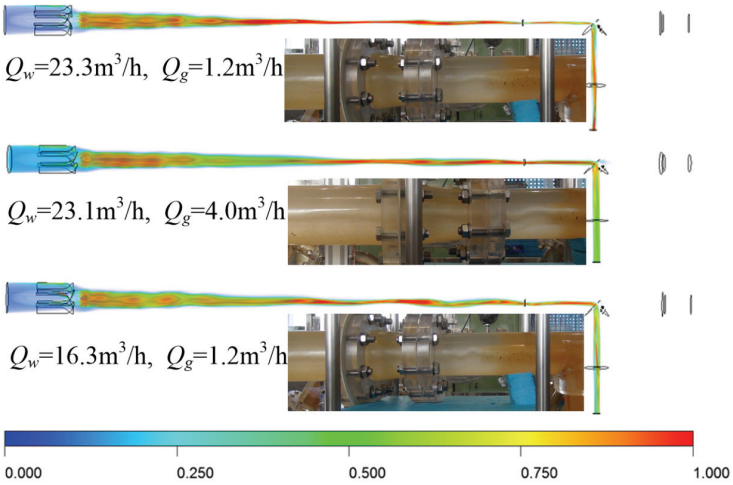

Figure 3. Comparison of numerical simulation with experiment of gas phase distribution under various operating conditions.

both numerical simulation and experimental observation show gas core in the separator. After flowing through the vane zone, bubble dispersion converges to be a gas core rapidly. Then, the gas core flows into phase collection equipment. Together with influence of pressure difference between branch and run outlet, gas core with possible liquids nearby flow out of the branch outlet. For each case, gas phase distribution through numerical simulation is in correspondence with experimental observation, both on tendency and gas core width.

Figure 4 presents void fraction distribution for 3 cases at the EIT testing section both numerically and experimentally at 6.0 s. In the figure, void fractions are measured and sampled radically. In subfigures (a), (b) and (c), the red hollow circle represents EIT measurement, with error bar included. The black hollow block represents simulation results. Generally speaking, high void fraction zone exists in the pipe center which means gas core both in simulation and experiment. It is obvious in each case that the void fraction curve trends are similar for simulation and experiment with nearly uniform peak value near 100% in the center. Difference lays in the gas core of the simulation, the result is thinner than the EIT measurement. This variation is acceptable considering resolution of EIT at gas-liquid surface.

As illustrated in Table 2, comparisons for split

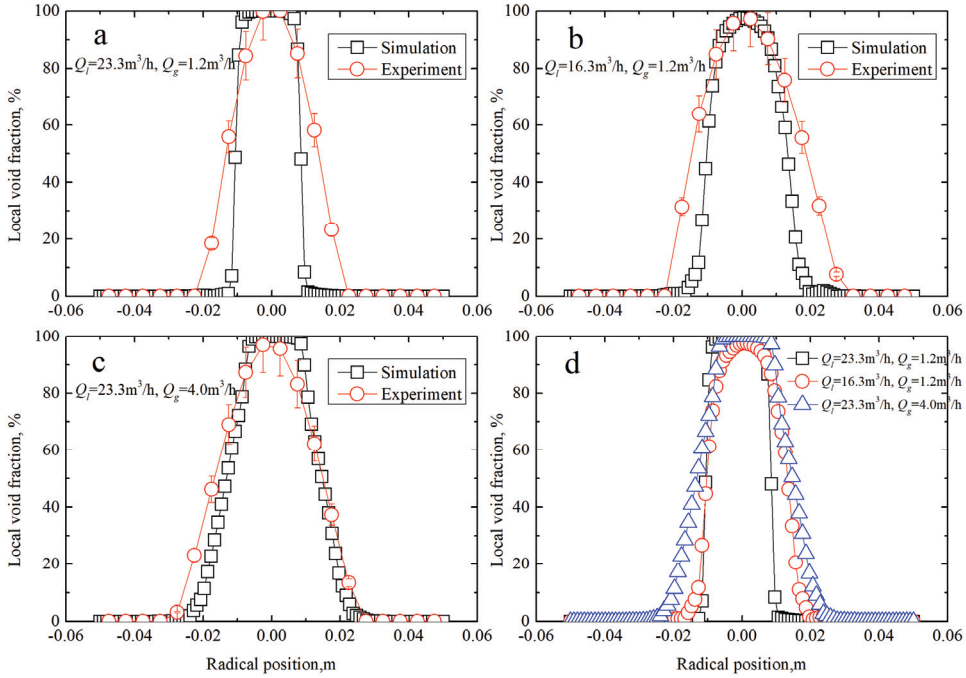

Figure 4. Void fraction distribution radically at 0.8 m downstream vane zone for various operating conditions.

ratio β between numerical simulation and experimental measurement are investigated. Here, split ratio β is defined by Eq. (7):

$$\beta = \frac{Q_{m\text{-}branch}}{Q_{m\text{-}inlet}} \tag{7}$$

in which $Q_{m\text{-}branch}$ and $Q_{m\text{-}inlet}$ are mixture flow rate of separator entrance and overflow, respectively. For cases 1 and 2, the relative errors are around 10%, and for case 3, the relative error is around 30%. Generally speaking, calculated split ratio is a bit higher than experimental measured ones. This may result from the simplification in the modeling procedure that regards the wall in the flow domain as a surface without thickness. Moreover, it seems that under high pressure difference between underflow and overflow, the numerical simulation is more accurate. Though variation between numerical and experimental split ratio exists, the discrepancy is acceptable for further analysis of the gas phase distribution in the separator.

The work in this subsection validates numerical simulation, which can be applied for detailed investigation of the gas-liquid swirling flow field investigation.

Gas phase distribution in the separator

Prior to research on separation performance, gas phase distribution in the separator should be investigated for the gas core's shape will influence gas flow rate entering gas collecting pipe which further influences separation performances.

When the phase inlet flow rate and split ratio is fixed, as is shown if case 1 (Q_w = 23.3 m^3/h and Q_g = = 1.2 m^3/h) in Figure 3, gas volume fraction contours are presented. In the contours, the red color represents high gas volume fraction, namely 1.0, and the blue color represents low gas volume fraction, namely 0.0, with other colors as transitions. It's obvious that the gas phase is evenly distributed before entering into the vane zone. After gas-liquid dispersion flows through the vane zone, the gas phase starts shrinking, a gas core with 100% gas phase is formed. Then the gas core flows into the phase collection branch and little left to the underflow. When it meets with the 90-degree elbow upstream of the overflow, due to abrupt change in flow direction, the gas core with continuous phase disintegrates to gas-water mixture, it has no influence on the separation performance.

When the gas inlet flow rate increases, and the split ratio rises, it comes to case 2 of Table 2. Compared with case 1, total gas core size is a bit wider in case 2. And the gas core is not as compact as case 1. On the basis of Liu *et al.* work [16], gas core in the flow field slashes swirl strength. Under higher inlet gas flow rate, lower swirl strength and larger gas flow rates make the gas core larger and less compact. Though higher split ratio may counteract this effect by creating a high-pressure difference which helps the gas core compact, it's a bit weak compared with large gas flow rate. On the basis of case 1, fixing inlet gas flow rate, lowing inlet liquid flow rate and split ratio, it turns into case 3. The gas core becomes wider and less compact as that of case 1. What's more, it takes more axial length for the gas core to be completely stable. It can be attributed to the lower swirling strength resulting from low inlet liquid flow rate and relatively high gas concentration.

Figure 4d further gathers radical void fraction distribution 0.8 m downstream vane zone for 3 cases. It's obvious that for all the 3 cases, the maximum of local void fraction reaches 100% near the pipe center. The difference lays in the width of the gas core. Case 1's gas core is the narrowest, and case 2's gas core is the widest. Another difference is the curves' shape near pipe center. curves of cases 1 and 3 are nearly flat, while case 2's shape is curved, with only the center point reaching 100%.

With fixed phase inlet flow rates and changed split ratio, as is shown in Figure 5, the gas core shape changes with split ratio. In Figure 5, the inlet liquid flow rate is 20.2 m^3/h, while the inlet gas flow rate is 4.0 m^3/h. As the split ratio increases from 22.9 to 33.6%, the gas core gradually becomes more constrained and thinner. Correspondingly, when fixing the split ratio and gas inlet flow rate with variation of inlet liquid flow rate, gas core shapes change as well. Figure 6 presents void fraction distribution measured by EIT 3000 0.8 m downstream vane zone under 3 dif-

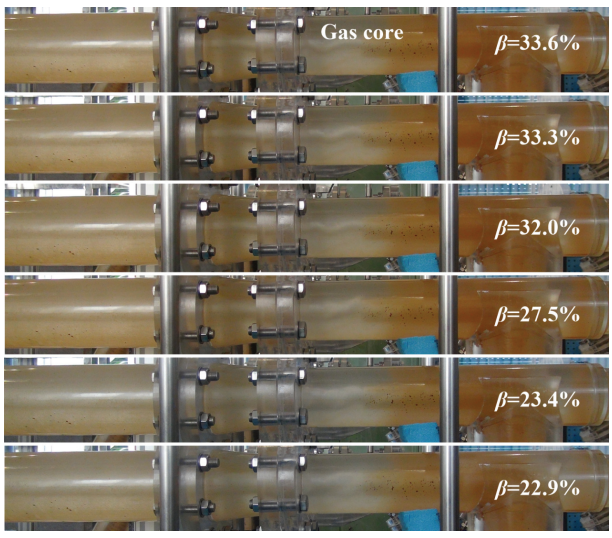

Figure 5. Gas phase distribution for various split ratios for 20.2 m^3/h liquid inlet flow rate and 4.0 m^3/h gas inlet flow rate.

ferent inlet liquid flow rates (13.3, 14.1 and 20.1 m^3/h) with red color representing high void fraction and blue color representing low void fraction. It can be seen that once split ratio and inlet gas flow rate are fixed, the gas core size is sensible to the inlet liquid flow rate. Gas core shrinks as inlet liquid flow rate increases. This is due to the fact that higher inlet flow rate aggravate radical acceleration which better promotes migration of the gas phase to the center and makes the gas core shrink. Considering the weakening effect of gas core on liquid phase continuity, all these in turn increase swirling strength by strengthening continuity of liquid phase. Hence, the gas core narrows as inlet liquid flow rate increases when inlet gas flow rate and split ratio are fixed.

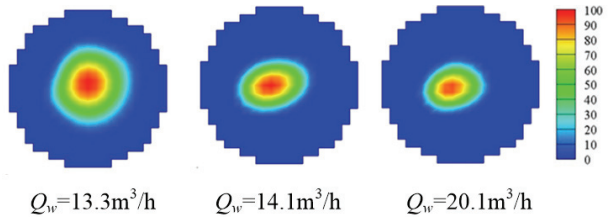

Figure 6. Void fraction distribution measured by EIT with 1.2 m^3/h gas inlet flow rate with 24% split ratio 0.8 m downstream vane zone.

Separation performances study

Separation performances are quantized by separation efficiency η, which is defined by ratio of gas flow rate of overflow and entrance as is shown in Eq. (8). In the equation, $Q_{g\text{-}branch}$ is the gas flow rate at overflow, and Q_g is the gas flow rate at entrance:

$$\eta = \frac{Q_{g\text{-}branch}}{Q_g} \tag{8}$$

Figure 7 presents separation efficiency variation with spilt ratio when one phase flow rate at the entrance is fixed. The data was obtained from experimental measurement of mixture density at outcome of separator by Coriolis mass flowmeter. Then the void fraction comes out through interpolation between gas and water density. Keeping inlet liquid flow rate at 20.2 m^3/h, a group of curves comes out for specific gas inlet flow rate. Each curve depicts separation efficiency under specific split ratio. Despite 6.0 m^3/h inlet gas flow rate, all the curves increase rapidly after first data is recorded. It means separation efficiency quickly rises beyond 97% and keeps nearly 100% as the split ratio increases. Unlike cases above, the rising trend is slower comparably for 4.0 m^3/h inlet gas flow rate conditions. Moreover, critical split ratio for separation efficiency to reach maximal rises as inlet gas flow rate increases as well. The reason for these phenomena is due to the gas core size compared with the phase collecting pipe diameter. For fixed inlet gas flow rates, higher split ratio results in lower overflow pressure which further compacts the gas core size and lets more gas phase flow through the overflow. As a consequence, separation efficiency increases. To discuss further, as inlet gas flow rates increase, the swirling strength decreases. As a result, larger split ratio is needed to create a larger pressure difference between the overflow and underflow to compact the gas core.

Comparably, as the inlet gas flow rate is fixed, a group of curves for different inlet liquid flow rate conditions comes out, which can be checked in Figure 7b. Separation efficiency rises much slower with the rise of split ratio in this situation. What's more, smaller split ratio is needed for separation efficiency, reaching maximum under high inlet liquid flow rate. These phenomena can be accumulated to gas core size and swirling strength as well. When the gas inlet flow rate is 4.0 m^3/h, the separation efficiency is not so sen-

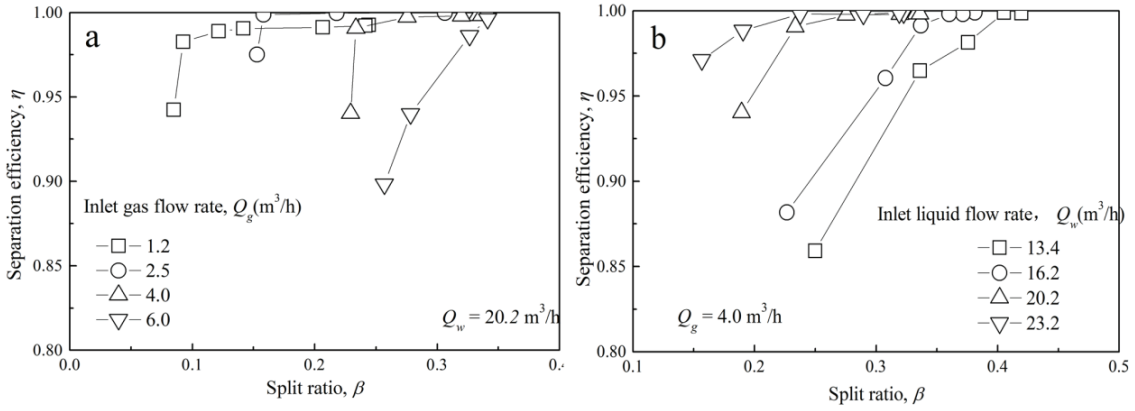

Figure 7. Variation of separation efficiency with split ratio under fixed inlet phase flow rate.

sible as it is at 20.1 m^3/h liquid inlet flow rate conditions. Besides, it needs a higher split ratio for lower liquid inlet flow rate conditions to form a strong enough swirling flow field which compacts the gas core size to achieve high separation efficiency.

CONCLUSION

This work concentrates on gas phase distribution and separation performances of a newly proposed vane-type separator with necking. ERT and numerical simulation were applied to conduct the research work. Conclusions are as follows:

Numerical simulation coupling Euler multiphase flow and RNG k-ε turbulent model is able to simulate the gas-liquid flow field.

The gas core size is sensible to operating parameters. Split ratio augments results in thinner gas core in fixed inlet phase flow rates. Increase of inlet liquid flow rate or decrease of inlet gas flow rate results in thinner gas core and vice versa.

The separator's performance is ideal, considering separation efficiency 85%, and can keep at nearly 100% after the adjustment of split ratio in all cases. Moreover, the separator performs relatively better at lower inlet gas flow rate and higher inlet liquid flow rate conditions.

The findings of this work extend the previous work to real separator design and performance investigation. It provides not only properties of the separator with specifications in this work, but also ways to systematically investigate a certain separator. Swirling vane, coupling necking in the developing tube, and phase collection tube mounted in the pipe center provide a prototype for a gas-liquid separator.

Acknowledgements

The authors gratefully acknowledge that the work described here is financially supported by Exploration and Development Area Optimization and Object Appraisal of Continental Shale Oil in Typical Basins in China (2017ZX05049) and the National Natural Science Foundation of China (No. 51779243).

Nomenclature

List of symbols

k	[J/kg]	turbulent kinetic energy
p_i	[Pa]	pressure of i^{th} phase
Q_w	[m^3/h]	liquid inlet flow rate
Q_g	[m^3/h]	gas inlet flow rate
$Q_{g\text{-}branch}$	[m^3/h]	gas flow rate at overflow
$Q_{m\text{-}inlet}$	[m^3/h]	mixture flow rate of entrance
$Q_{m\text{-}branch}$	[m^3/h]	mixture flow rate of overflow
$\bar{u}_i$	[m/s]	velocity of the i^{th} phase

Greek letters

α	[/]	local phase concentration
β	[/]	split ratio
ε	m^2/s^3	turbulent energy dissipation rate
η	[/]	separation efficiency
μ_a	[Pa.s]	viscosity of continuous phase
μ_b	[Pa.s]	viscosity of dispersed phase
μ_{ta}	[Pa.s]	continuous phase kinematic eddy viscosity
μ_{tb}	[Pa.s]	dispersed phase kinematic eddy viscosity
μ_w	[Pa.s]	water viscosity
ρ_a	[kg/m^3]	density of continuous phase
ρ_b	[kg/m^3]	density of dispersed phase
ρ_i	[kg/m^3]	density of i^{th} phase
ρ_w	[kg/m^3]	water density
σ_a	[/]	turbulent Prandtl number

REFERENCES

[1] A. Bahadori, Natural Gas Processing, Gulf Professional Publishing, Oxford, 2014, p. 181

[2] E.S. Rosa, F.A. França, G.S. Ribeiro, J. Pet. Sci. Eng. 32 (2001) 87-101

[3] R. Hreiz, R. Laine, J. Wu, C. Lemaitre, C. Gentric, D. Funfschilling, Int. J. Multiphase Flow 58 (2014) 15-26

[4] R. Hreiz, C. Gentric, N. Midoux, R. Lainé, D. Funfschilling, Chem. Eng. Res. Des. 92 (2014) 2231-2246

[5] S. Ohrem, T. Kristoffersen, C. Holden, Model-Based and Model-Free Optimal Control of a Gas Liquid Cylindrical Cyclone, in Proceedings of 3rd IFAC, Esbjerg, Denmark, 2018, p. 113

[6] J.A. Moncayo, R. Dabirian, R. Mohan, O. Shoham, G. Kouba, J. Pet. Sci. Eng. 165 (2018) 234-242

[7] S. Kanshio, H.Yeung, L. Lao, Flow Meas. Instrum. 53 (2017) 154-160

[8] B. Cai, J. Wang, L. Sun, N. Zhang, C. Yan, Prog. Nucl. Energy 74 (2014) 1-13

[9] L. Huang, S. Deng, C. Zhi, J. Guang, M. Chen, Sep. Purif. Technol. 194 (2017) 470-479

[10] L.A.C. Klujszo, P.K. Songfack, M. Rafaelof, R.K. Rajamani, Miner. Eng. 12 (1999) 1375-1392

[11] A.C. Hoffmann, W. Peng, H. Dries, M. Regelink, K. Foo, Energy Fuels 20 (2006) 1691-1697

[12] S.Y. Shi, J.Y. Xu, Exp. Therm. Fluid Sci. 60 (2015) 208--212

[13] H. Funahashi, K. Hayashi, S. Hosokawa, A. Tomiyama, Nucl. Eng. Des. 308 (2016) 205-213

[14] J.L. Yin, Y. Qian, Y.F. Ma, D.Z. Wang, Nucl. Eng. Des. 320 (2017) 133-140

[15] J.L. Yin, J.J. Li, Y.F. Ma, D.Z. Wang, Nucl. Sci. Tech. J. 8 (2015) 1-8

[16] S. Liu, L.L. Yang, D. Zhang, J.Y. Xu, Int. J. Multiphase Flow 107 (2018) 131-145

[17] S. Liu, D. Zhang, L.L. Yang, J.Y. Xu, Chem. Eng. Res. Des. 129 (2018) 35-54

[18] J.Z. Zhang, S. Liu, H. Li, X.P. Chen, J.W. Ma, J.Y. Xu, Chem. Eng. Commun. 205 (2018) 1351-1364

[19] X.P. Chen, Ph.D. Thesis, University of Chinese Academy of Sciences, Beijing, 2016, p. 47

[20] M. Brennan, Chem. Eng. Res. Des. 84 (2006) 495-505

[21] T. Neesse, J. Dueck, Miner. Eng. 20 (2007) 349-354

[22] A. Escue, J. Cui, Appl. Math. Modell. 34 (2010) 2840--2849

[23] M. Saidi., R. Maddahian, B. Farhanieh, Heat Mass Transfer 49 (2013) 247-260

[24] J. Serrano-Arellano, J.M. Riesco-Avila, J.M. Belman--Flores, K. Aguilar-Castro, E.V. Macias-Melo, Int. J. Heat Mass Transfer 102 (2016) 26-35

[25] M. Wang, R. Mann, F. Dickin, Chem. Eng. Commun. 175 (1999) 49-70.

JUN NIU[1]
SHUO LIU[2,3]
JING-YU XU[2,3]

[1]Petroleum Exploration and Production Research Institute of SINOPEC, Beijing, China
[2]Institute of Mechanics, Chinese Academy of Sciences, Beijing, China
[3]School of Engineering Sciences, University of Chinese Academy of Sciences, Beijing, China

NAUČNI RAD

ISTRAŽIVANJE EFIKASNOSTI RAZDVAJANJA CEVNOG SEPARATORA GAS-TEČNOST SA LOPATICAMA

U ovom radu pažljivo su istražene karakteristika raspodele gasne faze i efikasnost separacije novog separatora gas-tečnost sa lopaticama pomoću električne rezistentne tomografije i numeričke simulacije. Prečnik separatora je 100 mm, a protok se kreće u opsegu 12-23 m^3/h. Protok gasa je 1,2-4,0 m^3/h. Električna rezistentna tomografija je primenjena za istraživanje raspodele sadržaja gasa na probnom delu separatora. Coriolisov merač masenog protoka je korišćen da bi se odredila efikasnost razdvajanja faza mernjem gustine smeše na izlazu separatora. U numeričkoj simulaciji, primenjeni su puni Eulerov višefazni model, zajedno sa RNG k-ε turbulentnim modelom i bez dopunskih jednaćina za dispergovanu fazu. Rezultati pokazuju da na efikasnost separatora gas-tečnost sa lopaticama utiče veličina gasnog jezgra. Separator deluje dobro u svim slučajevima s obzirom na to da je efikasnost odvajanja veća od 85%, a postiže skoro 100% podešavanjem koeficijenta razdvajanja. Sva ova otkrića su korisna su projektovanje i optimizaciju separatora gas-tečnost sa lopaticams.

Ključne reči: razdvajanje gas-tečnost, efikasnost razdvajanja, numerička simulacija, cevni separator, projektovanje procesa.